Flow Instability for Binary Blends of Linear Polyethylene and Long-Chain Branched Polyethylene

Naoya Mieda and Masayuki Yamaguchi*

School of Materials Science,

Japan Advanced Institute of Science and Technology

1-1 Asahidai, Nomi, Ishikawa 923-1292 JAPAN

* Corresponding to

Masayuki Yamaguchi

School of Materials Science, Japan Advanced Institute of Science and Technology

1-1 Asahidai, Nomi, Ishikawa 923-1292 Japan

Phone +81-761-51-1621, Fax +81-761-51-1625

E-mail m_yama@jaist.ac.jp

Introduction

Control of rheological properties of molten polymers is one of the most important technologies for polymer processing [1-4]. For example, marked elastic natures such as normal stress difference, strain-hardening in elongational viscosity, and recoverable strain are required for the processing operations at which the deformation of a molten polymer with free surface occurs. In general, melt elasticity is pronounced by broadening molecular weight distribution and incorporation of long-chain branches. Therefore, low-density polyethylene (LDPE) produced by a radical polymerization method at high temperature and high pressure, that has broad molecular weight distribution and long-chain branches, shows good processability at foaming, blow-molding, film-blowing, and extrusion coating. Recently, however, it has been reported that melt elasticity of LDPE is enhanced by blending linear low-density polyethylene (LLDPE) or high-density polyethylene (HDPE), although both LLDPE and HDPE have narrow molecular weight distribution with no long-chain branches. This peculiar phenomenon was firstly reported by Utracki and Schlund under both shear flow [5] and extensional flow [6] employing LDPE/LLDPE blends. They found that zero-shear viscosity of the blends exhibits positive deviation from the log-additive rule. Later, Ajji et al. [7] found that LDPE/LLDPE blends containing 10-20 wt% of LDPE show marked strain-hardening behavior in elongational viscosity. Wagner et al. [8] also demonstrated that the strain-hardening behavior for LDPE/LLDPE is more pronounced than that for pure LDPE. Further, they discussed the growth curves of elongational viscosity quantitatively based on the molecular stress function theory. According to their study, addition of 5 wt% of LDPE provides the strain-hardening for LLDPE.

Furthermore, Lohse et al. [9] revealed that a blend composed of 3 wt% of a model comb-branch polyethylene and 97 wt% of LLDPE shows marked strain-hardening whereas the blend containing 3 wt% of a model star-branch polyethylene does not. Moreover, Delgadillo-Velazquez et al. [10] recently demonstrated that only 1 wt% of LDPE enhances the strain-hardening behavior.

The anomalous rheological properties are also detected for the blends with HDPE [11-13]. Furthermore, even LLDPE produced by metallocene catalyst having significantly narrow molecular weight distribution can enhance the drawdown force, defined as the force required for stretching a polymer melt, of LDPE [14-16]. Moreover, the anomalous rheological properties are marked for the blends with LDPE having well developed branch structure [10,17]. According to Wagner et al. [8], phase separation is the origin of the enhanced melt elasticity. However, recent our work revealed that the number of short-chain branches in a linear polyethylene, which affects the miscibility as shown by Lohse et al. from both theoretical and experimental approaches [18], has no/little influence on the anomalous rheological properties. Therefore, the blends with an ethylene-butene-1 copolymer (LLDPE) having a lot of short-chain branches (36 branches per 1000 backbone carbon atoms) show almost the same rheological properties as the blends with HDPE as far as the shear viscosity of the HDPE is the same level of the LLDPE [11,17,19]. The synenergetic properties were observed irrespective of the mixing method. Even the blends prepared by a twin-screw extruder exhibit marked elasticity [20,21], suggesting that the peculiar rheological properties are not attributed to the phase separation and/or poor mixing. Although it has been known that the number of short-chain branches has strong influence on the rubbery plateau modulus [22], flow activation energy [23,24], and the onset shear stress of shark-skin failure [25,26], the

effect is not so obvious as compared with the pronounced elastic properties of the blends. On the contrary, the molecular weight, i.e., shear viscosity, of a linear polyethylene plays an important role, on the rheological properties suggesting that entanglement couplings between LDPE and a linear polyethylene are responsible for the anomalous rheological responses [13,17,19]. The longest relaxation mechanism of the blends will be the relaxation of a backbone of branched chains in LDPE. In order to escape from a deformed tube by reptation, it has to drag the arm into the tube formed by the neighbor chains, i.e., arm retraction process [27]. In this case, primitive path fluctuation, dynamic tube dilation, and constraint release of branch parts become important, which have been proposed to predict the viscoelastic properties precisely by the tube model [25-29]. Since the primitive path fluctuation is affected by the length of a branch, the characteristic time of this motion is unchanged by blending LLDPE [28,30]. On the other hands, the characteristic times of the dynamic tube dilation and constraint release depend on the relaxation of surrounding chains. Consequently, the longest relaxation time of the blend with a linear polyethylene having high molecular weight becomes longer than that of the LDPE [31].

The mechanisms of the flow instability at capillary extrusion have been investigated for a long time [25,26,30-38]. It has been recognized that the flow instability can be classified into two types; one is rough surface, which is called as shark-skin failure, and the other is volumetric gross melt fracture. As the origin of shark-skin failure, two possible mechanisms have been proposed [39-42]. According to Cogswell [39], the origin of shark-skin is surface crack created by abrupt change in the boundary condition of tensile deformation in the vicinity of a die exit, which causes marked and sudden stretching of a surface layer of a melt. Another well-known

mechanism leading to the shark-skin is the slippage, i.e., adhesive failure, between a polymer melt and a die wall. Since it is generally accepted that a high viscous polymer melt slips on the wall, the slippage can be the origin of surface instability [35,43,44]. Gross melt fracture is attributed to the flow instability at a die entrance, and associated with long time relaxation mechanism [38,45-51]. Yamaguchi et al. found that gross melt fracture of LDPE can be avoided by applying intense shear history, which weakens the relaxation mechanism associated with long-chain branches, by shear modification [51]. Doelder and Koopmans reported that the critical conditions for the appearance of gross melt fracture depend on molecular mass and branching [47]. Meller et al. revealed that elongational stress decides the onset of gross melt fracture [38]. Flow instability for binary blends composed of LDPE and LLDPE or HDPE have been also investigated. Perez et al. found that blends containing a large amount of LDPE show gross melt fracture, whereas blending a small amount of LDPE can postpone the shark-skin failure for LLDPE [48]. Herranen and Savolaine also reported that addition of LDPE reduces the onset shear rate of shark-skin failure for LLDPE [49]. However, in many cases of the study on the flow instability for blends of LLDPE and LDPE, less attention has been paid on the anomalous rheological response such as marked melt elasticity to the best of our knowledge. Since the flow instability at capillary extrusion, as demonstrated by many researchers, is significantly sensitive to the rheological properties and thus the molecular structure of polymers, further investigation is required for the specific blend systems, especially binary blends of LDPE and LLDPE showing anomalous rheological response. Besides, it has to be understood also for the industrial application, because flow instabilities limit the productivity at actual processing operations.

In this paper, the flow instability at capillary extrusion is investigated employing

binary blends composed of LDPE, as a long-chain branched polyethylene, and three types of linear polyethylenes having different molecular weight. In particular, the effect of shear viscosity of the linear polyethylenes, which plays an important role on the anomalous behavior, on the flow instability at capillary extrusion is studied in detail. Since there have been poor study on the flow instability relating to the anomalous rheological response, it will be important information on actual processing operations.

Experimental

Materials

All samples employed in this study were commercially available materials. HDPE and two types of ethylene-1-hexene copolymers produced by metallocene catalyst were used as linear polyethylenes (L-PE). The number of the sample code denotes the value of the melt flow rate (MFR) at 190 ^{o}C. For example, L-PE-2 is the linear polyethylene whose MFR is 2 [g/10 min]. It should be noted that L-PE-20 has no short-chain branches (HDPE), whereas the others are ethylene-1-hexene copolymers. Further, LDPE produced by autoclave process was used as a long-chain branched polyethylene (B-PE). MFR of B-PE is 7.8 [g/10 min] at 190 ^{o}C.

The number-average molecular weight and weight-average molecular weight were determined by size elution chromatography, which are summarized in Table I. Furthermore, thermal properties such as crystallization temperature, melting point, and heat of fusion were examined by a differential scanning calorimeter at a heating/cooling rate of 10 ^{o}C/min. The results are shown in Table II. The melting point and the corresponding heat of fusion were measured for the samples cooled from 200 ^{o}C to

room temperature at a rate of 10 ^{o}C/min. In the table, information on short-chain branches is also provided. The number of short-chain branched was measured by Fourier-transfer Infra-red spectroscopy using the method proposed by Usami and Takayama [50]. Moreover, the apparent flow activation energy is evaluated by the rheological shift factors at various temperatures. As well known, the activation energy increases with increasing the number of short-chain branches as well as long-chain branches. According to Vega et al., [24] the activation energy (ΔH_a) for ethylene-α-olefin copolymer is provided as the following equation,

$$\Delta H_a = 23.8 + 26.7 \times \left[1 - \exp\left(-\frac{n}{35.4} \right) \right] \qquad (1)$$

where n is the number of short-chain branches per 1000 carbon atoms.

[Table I] [Table II]

Following eq. (1), L-PE-2 and L-PE-4 contain 20 and 21 short-chain branches per 1000 carbon atoms, respectively, which correspond well with the results obtained by FT-IR within the experimental error.

Sample Preparation

B-PE was mixed with one of the linear polyethylenes at various blend ratios in a laboratory-scale counter-rotating internal mixer with blade-type rotors at 230 ^{o}C (Toyoseiki, Labo-plastmil) with calcium stearate as a neutralizer and pentaerythritol tetrakis(3-3,5-di-tert-butyl-4-hydroxyphenyl) propionate (Ciba, Irganox1010) and tris(2,4-di-tert-butylphenyl)phosphate (Ciba, Irgafos168) as thermal stabilizers. Further, The amount of the total polyethylene was 48 g, i.e., full-filling condition, in order to mix the materials homogeneously. The blade rotation speed was 30 rpm and the mixing

time was 3 min. Further, the same processing history was applied to the individual pure components. The obtained samples were compressed into a flat sheet by a compression-molding machine at 230 ^{o}C for 10 min and then subsequently cooled down at 30 ^{o}C. In this study, the mixing and processing protocol were determined in order to avoid the effect of the applied mixing histories on the rheological properties during measurements, because rheological properties of LDPE and blends with LDPE are sensitive to processing history, which is known as shear modification [13,51].

Measurements

The frequency dependence of oscillatory shear modulus in the molten state was measured by a cone-and-plate rheometer (UBM, MR500) at various temperatures under a nitrogen atmosphere.

The drawdown force, defined as the force required for extension of a polymer melt, was evaluated at 160 ^{o}C by a capillary rheometer (Yasuda Seiki Seisakusyo, 140 SAS-2002) equipped with a capillary die of 8 mm in length and 2.095 in diameter, having $\pi/2$ entrance angle. The extruded strand was pulled downward by a set of rotating wheals. In this experiment, the drawdown force was evaluated at a draw ratio of 7.

The growth curves of uniaxial elongational viscosities were measured by a Sentmanat Extension Rheometer (SER) (Xpansion Instruments, LLC) designed for use as a detachable extensional rheometer fixture on commercially available torsional rheometer systems (TA instruments, AR2000).

Capillary extrusion was performed by the capillary rheometer at 160 ^{o}C to evaluate the steady-state shear viscosity and the appearance of extrudates. A circular die

having L/D=20/1 (mm) was employed. Moreover, other circular dies having L/D=10/1 (mm) and L/D=40/1 (mm) were also employed to evaluate the end pressure drop.

Results and Discussion

Oscillatory Shear Modulus

The master curves of frequency dependence of shear storage modulus *G'* and loss modulus *G"* for B-PE/L-PE-4 blends are exemplified in Figure 1 without vertical shift. The reference temperature is 160 ^{o}C. As seen in the figure, the time-temperature superposition principle is not applicable to B-PE and some blends. The phenomenon has been already reported and believed to be attributed to the difference of flow activation energy of the relaxation mechanism associated with long-chain branches [8,9]. Moreover, B-PE shows higher moduli than L-PE-4 in the low frequency region and lower moduli in the high frequency. This is reasonable because B-PE has broad distribution of relaxation time due to the broad molecular weight distribution and long-chain branches. Furthermore, it should be noted that blending L-PE-4 enhances the moduli to a great extent in the low frequency region. In particular, the oscillatory shear moduli for B-PE/L-PE-4 (75/25) and B-PE/L-PE-4 (50/50) are almost the same as those for pure B-PE in the low frequency region.

Figure 2 represent the master curves of shear storage modulus *G'* and loss modulus *G"* for B-PE/L-PE-2 blends. As seen in the figure, the blends show higher moduli than B-PE/L-PE-4 blends. In particular, the oscillatory moduli for B-PE/L-PE2 (25/75) and (50/50) are higher than those for pure B-PE in the low frequency region.

[Figure 1][Figure 2]

The synergetic phenomenon of the blends is clearly demonstrated in the plot of zero-shear viscosity, calculated by G", as shown in Figure 3. Although some samples exhibit thermorheological complexity, the values can be evaluated within the experimental error. It is apparent from the figure that the data of the blends with L-PE having high shear viscosity, such as L-PE-2 and L-PE-4, deviate from the log-additive rule. On the contrary, those of the blends with L-PE having low shear viscosity, i.e., L-PE-20, follow the log-additive rule as shown in some miscible blend systems [52,53]. Considering that the zero-shear viscosity η_0 is expressed in eq. (2), the blends whose zero-shear viscosities are higher than those of the individual components have long relaxation time τ and/or large value of relaxation spectra $H(\tau)$.

$$\eta_0 = \int_{-\infty}^{\infty} \tau\, H(\tau)\, d \ln \tau \qquad (2)$$

Assuming that the system is a homogeneous melt as suggested in our previous paper [17], the entanglement couplings having a long characteristic time, which is probably ascribed to the relaxation of backbone of branched chains in B-PE, are enhanced in the anomalous blends.

[Figure 3]

Rheological Response under Elongational Flow

Since uniaxial elongational viscosity is sensitive to long time relaxation mechanism, especially that ascribed to long-chain branches, the synergetic effect of the blend systems is pronounced for the rheological response under elongational flow. Figure 3 shows the drawdown force, which has a close relationship with elongational viscosity [51], plotted against the weight fraction of L-PE. It is found from the figure

that the drawdown force for the blends with L-PE-20 follows the linear additive rule. However, the data of the blends with L-PE-2 apparently deviate from the linear additive rule. For example, the drawdown force of B-PE/L-PE-2 (50/50), 170 mN, is significantly higher than that of pure B-PE, 90 mN. Because the blend shows almost the same level of the oscillatory shear moduli, i.e., viscoelastic response in the linear region, as pure B-PE, the marked deviation of the drawdown force is attributed to the strain-hardening behavior in transient uniaxial elongational viscosity as shown later.

[Figure 4]

Growth curves of elongational viscosity measured at 160 ^{o}C at various strain rates for B-PE, L-PE-2, and their blends are shown in Figure 5. The solid line in the figure represents $3\eta^{+}(t)$, where $\eta^{+}(t)$ is a growth curve of shear viscosity at a low shear rate asymptote. The value is calculated from the oscillatory shear moduli using eq. (3) proposed by Osaki et al. [55];

$$\eta^{+}(t) = t\left[G''(\omega) + 1.12G'(\omega/2) - 0.200G'(\omega)\right]\Big|_{\omega\to\frac{1}{t}} \quad (3)$$

As seen in the figure, B-PE shows marked strain-hardening behavior as compared with L-PE-2 even though MFR of L-PE-2 is lower than that of B-PE. Further, it should be noted that the degree of strain-hardening behavior is pronounced for the blends with L-PE-2. For example, B-PE/L-PE-2 (50/50) shows more pronounced strain-hardening than B-PE. Moreover, the blend with only 25 wt% of B-PE shows a similar level of the strain-hardening to B-PE.

[Figure 5]

Elongational viscosity of the other blends cannot be obtained because of the difficulty of the measurements.

Capillary Extrusion

The flow curves without Bagley and Rabinovitsch corrections of B-PE, L-PE, and the blends, measured by the capillary rheometer at 160 ^{o}C, are shown in Figure 6. Shear stress of B-PE is higher than that of L-PE-20, whereas L-PE-2 and L-PE-4 show lower viscosity than B-PE. In the experimental shear rate range, the slope of B-PE is lower than those of L-PE, which is attributed to the broad distribution of relaxation time. Further, it seems that the shear stress of the blends with L-PE-20 follows log-additive rule. On the contrary, the blends with L-PE having high shear viscosity deviate from the log-additive rule. Moreover, the shear stress of L-PE-2 at high shear rate region is almost independent of the shear rate. In this region, slippage at the capillary wall must take place to some degree. For example, the slip-stick phenomenon, which is typical flow instability for L-PE, occurs at 560 s^{-1}. Because of the slip-stick failure, the stress oscillates from 0.332 to 0.371 MPa.

[Figure 6]

The photographs of the extruded stands are shown in Figure 7. In case of the blends with L-PE-2 and L-PE-4, the diameter of strands is significantly larger than that of pure LDPE. The marked Barus effect is explained by the enhanced elastic nature. Further, it is found from the figure that B-PE exhibits gross melt fracture at 560 s^{-1} with smooth surface, whereas all L-PE samples do not show gross melt fracture even at the highest shear rate in this experiment. The shark-skin failure is detected for B-PE/L-PE-4 (25/75) at 560 s^{-1} and B-PE/L-PE-2 (25/75) at 150 s^{-1}. In case of pure L-PE, the shark-skin failure is not detected even by a scanning electron microscope, although L-PE-2 shows the slip-stick failure at 560 s^{-1}. The onset stress of the shark-skin failure

must be higher than the stress at the current experimental condition, suggesting that the blends exhibit lower onset stress.

It should be noted that the onset stress of the shark-skin failure for the blends with L-PE-2 and L-PE-4 clearly decreases by blending B-PE. In particular, L-PE-2/B-PE (75/25) shows the shark-skin failure at low shear stress (0.257 MPa). Moreover, it is apparent that the blends with L-PE-2 or L-PE-4 exhibit severe gross melt fracture with rough surface at high shear rate region. These experimental results suggest that the blends showing marked melt elasticity tend to exhibit severe flow failures easily.

[Figure 7]

Recently, Yamaguchi et al. [25] demonstrated that the steady-state shear stress is expressed by the relaxation time distribution, Deborah number, and rubbery plateau modulus as shown in eq. (4) based on the Carreau equation proposed for a generalized Newtonian fluid (eq. (5)),

$$\sigma(\dot{\gamma}) = \left(\frac{\tau_w}{\tau_n}\right)^{n-1} De^n \, G_N^0 \qquad (4)$$

$$\sigma(\dot{\gamma}) = \dot{\gamma}\,\eta_0\left[1+(\tau_w\dot{\gamma})^2\right]^{\frac{n-1}{2}} \qquad (5)$$

where τ_n and τ_w the number and weight average relaxation times, *De* the Deborah number, n (<1) the constant which is the function of molecular weight distribution, and G_N^0 the rubbery plateau modulus.

Since G_N^0 is assumed to be a constant, broad distribution of relaxation time leads to large *De* at the same shear stress. It is apparent that the relaxation time distribution of the blends showing high η_0 is significantly broader than that of a pure linear polyethylene because of the following reasons; (1) B-PE has broad distribution of

relaxation time and (2) long time relaxation mechanism is pronounced for the blend systems because constraint release and dynamic tube dilation processes are reduced to some degree by existence of high molecular weight fraction as surrounding chains. The origins of the shark-skin failure have been studied for a long time and believed to be surface crack and/or slippage at the wall. Both failures occur at high Deborah number condition, because polymer melts store large energy during flow like elastic solids. Therefore, the shark-skin failure is detected at low shear stress for the blends showing synergetic phenomenon.

As demonstrated, severe gross melt fracture is detected for the blends showing high level of drawdown force. The origin of the gross melt fracture is believed to be flow instability at the die entrance. Meller et al. [38] found that elongational stress generated by contraction flow at the die entrance decides the occurrence of gross melt fracture. Since long-chain branched polymers exhibit marked strain-hardening in elongational viscosity, leading to high elongational stress, gross melt fracture is always detected. As shown in Figure 4, the drawdown force of the blends with L-PE-4 or L-PE-2, is higher than that of pure B-PE. This is one of the reasons of severe gross melt fracture observed in the blends.

At capillary extrusion of branched polymers having high melt elasticity, flow behaviors around the die entrance, especially entrance angle, has to be considered carefully, because the entrance angle determines the actual elongational strain rate by the contraction flow, and thus, the elongational stress. It has been known that an entrance angle of LDPE is small because of the occurrence of vortices, whereas that of LLDPE and HDPE is large. Lamb and Cogswell [56] proposed the following empirical relation considering that polymer melts showing high level of elongational viscosity

favors a low elongational strain rate as follows;

$$\alpha = \tan^{-1} \frac{2\eta}{\eta_E} \qquad (6)$$

where η and η_E are the shear and elongational viscosities.

The entrance angle of the blend systems composed of B-PE and L-PE with high shear viscosity is, however, unrevealed, although it is important information to understand the gross melt fracture. In this study, the entrance angle is predicted by the method proposed by Ballerger and White [57]. According to them, the entrance angle α is related to the ratio of the end pressure drop ΔP_e to the wall shear stress σ_w as shown in the following equation.

$$\alpha = 178.5(0.9644)^{\Delta P_e / \sigma_w} \qquad (7)$$

Although this empirical relation has no theoretical background, it has been proved that many data follow eq. (7) [57].

Figure 8 presents the magnitude of ΔP_e plotted against the L-PE content at various shear rates for L-PE-2/B-PE blends. It is generally understood that ΔP_e is composed of viscous and elastic components. Therefore, ΔP_e of a polymer melt with marked elastic property is higher than that of a polymer with poor melt elasticity as long as both polymers show the same shear viscosity. It is found from the figure that some blends show higher ΔP_e than pure B-PE. The results are reasonable because the blends with L-PE having high shear viscosity exhibit marked melt elasticity.

[Figure 8][Figure 9]

Figure 9 shows the entrance angle α calculated from eq. (7) as a function of the shear rate. As seen in the figure, the entrance angle decreases with increasing the shear rate. Further, the entrance angle decreases with increasing the B-PE content

monotonically, suggesting that the entrance angle does not show synergetic effect. Consequently, the actual elongational strain rate at the die entry of the blends is higher than that of pure B-PE at the same volume flow rate. Since the elongational viscosity of the blend is higher than that of B-PE, eq. (6) is not applicable to the system. Further, these results suggest that the blends showing marked strain-hardening in elongational viscosity flow at the die entrance at a high elongational strain rate as compared with B-PE. As a result, the difference in elongational stress is magnified, leading to severe gross melt fracture for the blends.

Conclusion

Flow instability at capillary extrusion is studied employing binary blends composed of a linear polyethylene (L-PE) and a long-chain branched polyethylene (B-PE). As already reported, the blends containing L-PE with high shear viscosity exhibit synergetic effect, e.g., enhanced zero-shear viscosity and marked strain-hardening behavior in elongational viscosity. The blends showing the anomalous rheological response exhibit shark-skin failure at low shear stress as compared with pure L-PE. The phenomenon is explained by the high Deborah number for the blends. Moreover, the blends show severe gross melt fracture as compared with B-PE. Enhanced strain-hardening in elongational viscosity and large entrance angle at the die entry will be responsible for the gross melt fracture for the blends.

Reference

[1] V.R. Kuhn, H. Kromer, G. Rosmanith, Struktur und eigenschaften verschieden hergestellter hochdruckpolyäthylene, Angew. Makromol. Chem. 40 (1974) 361-389.

[2] T.G. Schole, N.L.J. Meijerink, Analysis of heterogeneity by sedimentation transport: Concentration and pressure effects, Br. Polym. J. 6 (1974) 133-142.

[3] V.R Kuhn, H. Kromer, Structures and properties of different low density polyethylenes, Colloid Polym. Sci. 260 (1982) 1083-1092.

[4] Z. Tadmor, C.G. Gogos Principles of polymer processing. Willy-Interscience, 2006

[5] L.A. Utracki, B. Schlund, Linear low density polyethylenes and their blends: Part 4 shear flow of LLDPE blends with LLDPE and LDPE, Polym. Eng. Sci. 27 (1987) 1512-1522.

[6] B. Schlund, L.A. Utracki, Linear low density polyethylenes and their blends: Part 5 extensional flow of LLDPE blends, Polym. Eng. Sci. 27 (1987) 1523-1529.

[7] A. Ajji, P. Sammut, M.A. Huneault, Elongational rheology of LLDPE / LDPE blends, J. Appl. Polym. Sci. 88 (2003) 3070-3077.

[8] M.H. Wagner, S. Kheirandish, M. Yamaguchi, Quantitative analysis of melt elongational behavior of LLDPE/LDPE blends, Rheol. Acta. 44 (2004) 198-218.

[9] D.J. Lohse, S.T. Milner, L.J. Fetters, M. Xenidou, N. Hadjichristidis, R.A. Mendelson, C.A. Garcia-Franco, M.K. Lyon, Well-defined model long chain branched polyethylene 2. Melt rheological properties, Macromolecules 35 (2002 3066-3075.

[10] O. Delegadillo-Velazquez, S.G. Hazikirakos, M. Sentmanat, Thermorheological properties of LLDPE/LDPE blends, Rheol. Acta. 47 (2008) 19-31.

[11] A. Valenza, F.P.L. Manitia, D. Acierno, The rheological behavior of HDPE/LDPE blends. V. isothermal elongation at constant stretching rate, J. Rheol. 30 (1986) 1085-1092.

[12] A. Ghijsels, J.J.S.M. Ente, J. Raadsen, Melt Strength Behavior of Polyethylene Blends, Int. Polym. Process. 7 (1992) 44-50.

[13] M. Yamaguchi, Relationship between processing history and rheological properties during postprocessing annealing for anomalous polyethylene blends, J. Appl. Polym. Sci. 102 (2006) 1078-1083.

[14] T. Hameed, I.A. Hussein, Rheological study of the influence of Mw and comonomer type on the miscibility of m-LLDPE and LDPE blends, Polymer 43 (2002) 6911-6929.

[15] I.A. Hussein, T. Hameed, B.F.A. Sharkh, K. Mezghani, Miscibility of hexene-LLDPE and LDPE blends: Influence of branch content and composition distribution, Polymer 44 (2003) 4665-4672.

[16] I.A. Hussein, M.C. Williams, Rheological study of the influence of branch content on the miscibility of octene m-LLDPE and ZN-LLDPE in LDPE, Polym. Eng. Sci. 44 (2004) 660-672.

[17] N. Mieda, M. Yamaguchi, Anomalous rheological response for binary blends of linear polyethylene and long-chain branched polyethylene, Adv. Polym. Technol. 26 (2007) 173-181.

[18] D. R. Raul, C. B. Bucknall, Polymer Blends 2nd Edition, Chap 8, Thermodynamics of polyolefine blends, D. J. Lose and W. W. Graessly, Wiley New York, 1990.

[19] M. Yamaguchi, Anomalous rheological properties of polyethylene molecular composites, Polymer Eng. Sci. 46 (2007) 1284-1291.

[20] P. Micic, S.N. Bhattacharya, G. Field, Rheological behavior of LLDPE/LDPE blends under elongational deformation, Int. Polym. Process. 12 (1997) 110-115.

[21] P. Micic Transient elongational viscosity of LLDPE/LDPE blends and its Rrlevance to bubble stability in the film blowing process, Polym. Eng. Sci. 38 (1998) 1685-1693.

[22] H. Miyata, M. Yamaguchi, M. Akashi, Structure and viscoelastic properties of amorphous ethylene/1-hexene copolymers obtained with metallocene catalyst, Polymer 42 (2001) 5763-5769.

[23] F.J. Stadler, C. Gabriel, H. Münstedt, Influence of short-chain branching of polyethylenes on the temperature dependence of rheological properties in shear, 208 (2007) 2449-2454.

[24] J. F. Vega and A. Santamaría, Small-amplitude oscillatory shear flow measurements as a tool to detect very low amounts of long chain branching in polyethylenes, Macromolecules, 31 (1998) 3639-3647.

[25] M. Yamaguchi, H. Miyata, V. Tan, C.G. Gogos, Relation between molecular structure and flow instability for ethylene/α-olefin copolymers, Polymer 43 (2002) 5249-5255.

[26] A. Allal, B. Vergnes, Molecular design to eliminate sharkskin defect for linear polymers, J. Non-Newtonian Fluid Mech. 146 (2007) 45-50.

[27] M. Doi, S.F. Edward, The Theory of Polymer Dynamics Clarendon Press, Oxford 1986.

[28] M. Doi, Explanation for the 3.4 power law of viscosity of polymeric liquids on the basis of the tube model, J. Polym. Sci.-Phys. 21 (1983) 667-684.

[29] H. Watanabe, S. Ishida, Y. Matsumiya, T. Inoue, Test of Full and Partial Tube Dilation Pictures in Entangled Blends of Linear Polyisoprenes, Macromolecules 37 (2004) 6619-6631.

[30] S.T. Milner, T.C.B. MacLeish, Reptation and contour-length fluctuation in melts of linear polymers, Phys. Rev. Lett. 81 (1998) 725-728.

[31] W.H. Tuminello, Molecular-weight polydispersity effects on the viscoelasticity of entangled linear-polymers, Polym. Eng. Sci. 26 (1986) 1339-1347.

[32] J. Tordella, Unstable flow of molten polymers: a second site of melt fracture, J. Appl. Phys. 7 (1963) 215-229.

[33] F. Cogswell, Stretching flow instabilities at the exits of extrusion dies, J. Non-Newtonian Fluid Mech. 2 (1977) 37-47.

[34] C. Tu C, Melt rheology of semirigid PVC compounds, J. Vinyl Technol. 2 (1980) 240-243.

[35] D. Kalika, M.M. Denn Wall slip and extrudate distortion in linear low-density polyethylene, J. Rheol. 31 (1987) 815-834.

[36] C. Deeprasertkul, Molecular character of sharkskin phenomenon in metallocene linear low density polyethylenes, Macromol. Chem. Phys. 199 (1998) 2113-2118.

[37] V. Mhetar, Slip in entangled polymer melts. 1. General Features, Macromolecules 31 (1998) 8607-8616.

[38] M. Meller, A. Luciani, A. Sarioglu, J.E. Manson, Flow through a convergence part 1: Critical conditions for unstable flow, Polym. Eng. Sci. 42 (2002) 611-633.

[39] F. N. Cogswell, Polymer Melt Rheology; George Godwin Ltd., London, 1981.

[40] J.M. Dealy, K.F. Wissbrun, Melt Rheology and Its Role in Plastics Processing; Van Nostrand Reinhold: New York, 1989.

[41] J.M. Piau, J.F. Agassant, Rheology for Polymer Melt Processing; Elsevier: Amsterdam, 1996.

[42] S.G. Hatzikiriakos, K.B. Migler, Polymer Processing Instabilities; Marcel Dekker: New York, 2005.

[43] A.V. Ramanathy, Wall slip in viscous fluids and influence of materials of construction, J. Rheol. 30 (1986) 337-358.

[44] V.G. Ghanta, B.L. Riise, M.M. Denn, Disappearance of extrusion instabilities in brass capillary dies, J. Rheol. 43 (1990) 435-443.

[45] J.L. White, Critique on flow patterns in polymer fluids at the entrance of a die and instabilities leading to extrudate distortion, Appl. Polym. Symp. 20 (1983) 155-174.

[46] M Yamuguchi, Flow instability in capillary extrusion of plasticized poly(vinyl chloride), J. Appl. Polym. Sci. 82 (2001) 1277-1283.

[47] J. Doelder, R. Koopmans, Pressure oscillations and periodic extrudate distortions of long-chain branched polyolefins, J. Rheol. 49 (2005) 113-126.

[48] R. Perez, E. Rojo, M. Fernandez, V. Leal, P. Lafuente, A. Santamaria, Basic and applied rheology of m-LLDPE/LDPE blends: Miscibility and processing features, Polymer 46 (2005) 8045-8053.

[49] M. Herranen and A. Savolainen, Correlation between melt fracture and ultrasonic velocity, Rheol. Acta. 23 (1984) 461-464.

[50] T. Usami, and S. Takayama, Identification of Branches in Low-Density Polyethylenes by Fourier Transform Infrared Spectroscopy, 16 (1984) 731-738.

[51] M. Yamuguchi, D.B. Todd, C.G. Gogos, Rheological properties of LDPE processed by conventional processing machines, Adv. Polym. Technol. 22 (2003) 179-183.

[52] L.A. Utracki, Polymer alloys and blends, Thermodynaqmics and rheology. Hanser, Munich, 1989.

[53] M. Yamaguchi, H. Miyata, K. Nitta, T. Masuda, Rheological properties for binary blends of i-PP and ethylene-1-hexene, J. Appl. Polym. Sci. 63 (1997) 467-474.

[54] A. Bernnat, Polymer melt rheology and the rheotens test. Dr. Thesis, Univ. Stuttgart, 2001.

[55] K. Osaki, A. Murai, N. Bessho, B.S. Kim, Linear Viscoelastic relation concerning shear stress at the start and cession of steady shear flow, J. Soc. Rheol. Jpa. 4 (1976) 166-169

[56] P. Lamb, F.N. Cogswell, International plastics congress on processing polymer products, Amsterdam, 1966.

[57] T.F. Ballenger, J.L. White, The development of the velocity field in polymer melts into a reservoir approaching a capillary die, J. Appl. Polym. Sci. 15 (1971) 1849-1962.

Figure caption

Fig. 1 Master curves of frequency dependence of (a) shear storage modulus G' and (b) loss modulus G'' for B-PE/L-PE-4 blends at 160 ^{o}C; (■) B-PE, (Δ) B-PE/L-PE-4 (75/25), (□) B-PE/L-PE-4 (50/50), (Δ) B-PE/L-PE-4 (25/75), and (●) L-PE-4.

Fig. 2 Master curves of frequency dependence of (a) shear storage modulus G' and (b) loss modulus G'' for B-PE/L-PE-2 blends at 160 ^{o}C; (■) B-PE, (Δ) B-PE/L-PE-2 (75/25), (□) B-PE/L-PE-2 (50/50), (Δ) B-PE/L-PE-2 (25/75), and (●) L-PE-2.

Fig. 3 Zero-shear viscosity of B-PE/L-PE blends at 160 ^{o}C; (●) B-PE/L-PE-20, (▲) B-PE/L-PE-4, and (■) B-PE/L-PE-2.

Fig. 4 Drawdown force of B-PE/L-PE blends at 160 ^{o}C; (●) B-PE/L-PE-20, (▲) B-PE/L-PE-4, and (■) B-PE/L-PE-2 blends.

Fig. 5 Growth curves of elongational viscosity at 160 ^{o}C; (a) B-PE, (b) B-PE/L-PE-2 (75/25), (c) B-PE/L-PE-2 (50/50), (d) B-PE/L-PE-2 (25/75), and (e) L-PE-2 at various strain rates; (▽) 0.72 s^{-1}, (△) 0.36 s^{-1}, (◇) 0.18 s^{-1}, (□) 0.09 s^{-1} and (○) 0.05 s^{-1}. The solid line denotes the growth curve of elongational viscosity at a low strain rate asymptote.

Fig 6 Flow curves of (a) B-PE/L-PE-20 blend at 160 ^{o}C; (●) B-PE, (○) B-PE/L-PE-20 (75/25), (Δ) B-PE/L-PE-20 (50/50), (□) B-PE/L-PE-20 (25/75), and (▲) L-PE-20, (b) B-PE/L-PE-4 blend at 160 ^{o}C; (●) B-PE, (○) B-PE/L-PE-4 (75/25), (Δ) B-PE/L-PE-4 (50/50), (□) B-PE/L-PE-4 (25/75), and (▲) L-PE-4, (c) B-PE/L-PE-2 blend at 160 ^{o}C; (●) B-PE, (○) B-PE/L-PE-2 (75/25), (Δ) B-PE/L-PE-2 (50/50), (□) B-PE/L-PE-2 (25/75), and (▲) L-PE-2.

Fig. 7 Optical photographs of extruded stands at 160 ^{o}C. A circular die having L/D=20/1 (mm) was employed; (a) B-PE/L-PE-20, (b) B-PE/L-PE-4, and (c) B-PE/L-PE-2. The numerals in the figure represent the apparent shear stress (MPa).

Fig. 8 End pressure loss (ΔPe) for B-PE/L-PE-2 blends at various shear rates at 160 ^{o}C; (●) 15 s^{-1}, (■) 35 s^{-1}, and (▲) 75 s^{-1}.

Fig. 9 Entrance angle of B-PE/L-PE-2 blends with various L-PE-2 contents at 160 ^{o}C; (●) B-PE, (■) B-PE/L-PE-2 (75/25), (♦) B-PE/L-PE-2 (50/50), (▼) B-PE/L-PE-2 (25/75), and (▲) L-PE-2.

Table 1. Molecular characteristics of polymers

	Molecular weights		Number of SCB	Density
	Mn $\times 10^{-4}$	Mw $\times 10^{-4}$	(per 1000 carbon atoms)	(kg/m^3)
B-PE	1.4	14	32	917
L-PE-2	11	23	22	913
L-PE-4	8.1	18	23	904
L-PE-20	0.8	6.4	—	968

Table 2. Thermal and flow characteristics of polymers

	Melt index (g/10 min)	Thermal properties		ΔH_a (kJ/mol)
		T_m (^oC)	ΔH_F (J/g)	
B-PE	7.2	106.8	105.6	52.8
L-PE-2	2.0	112.8	88.1	31.0
L-PE-4	3.8	112.5	76.4	31.2
L-PE-20	20	135.2	227.6	25.7

Fig. 1 (a)

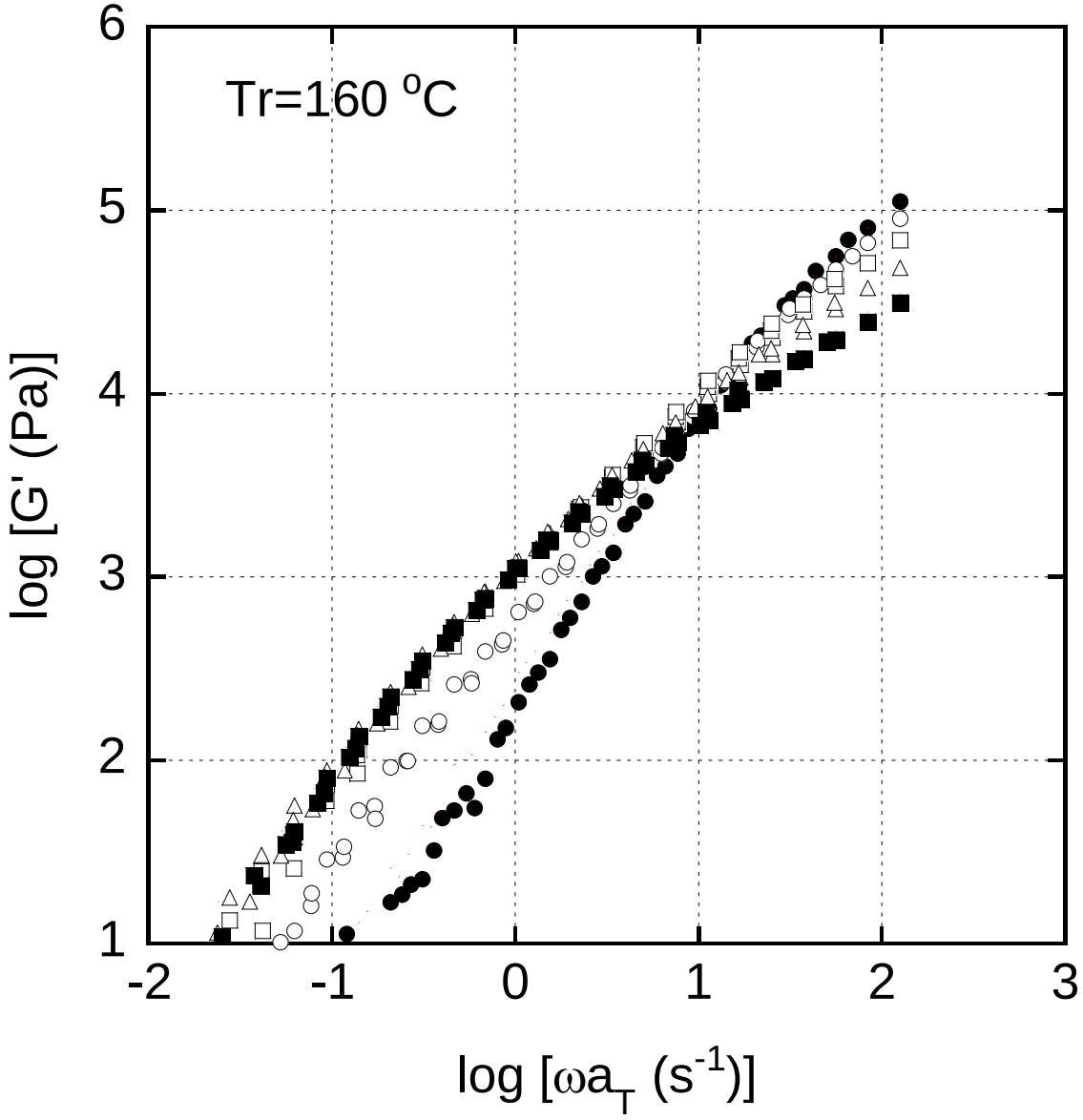

Fig. 1 (b)

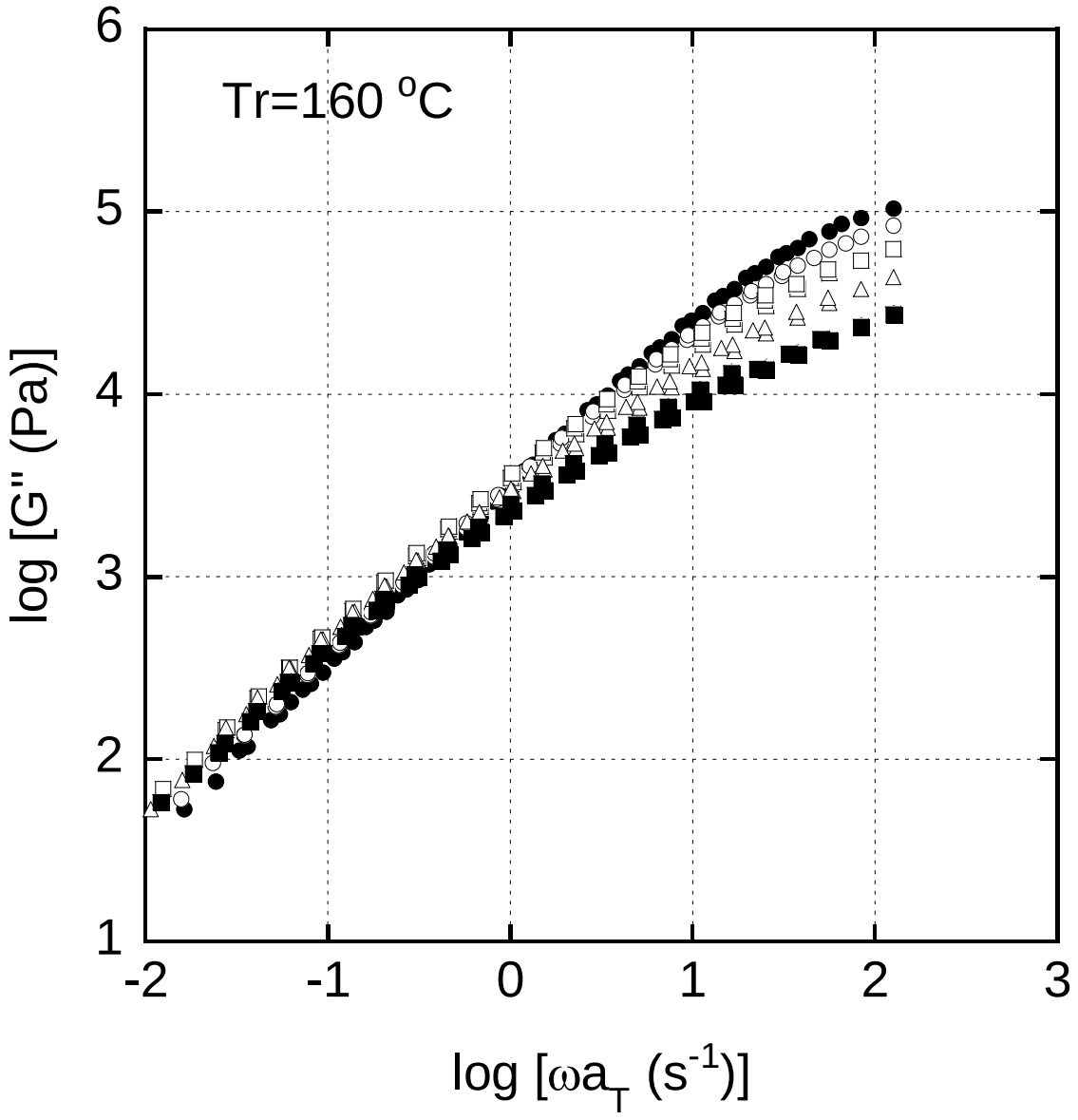

Fig. 2 (a)

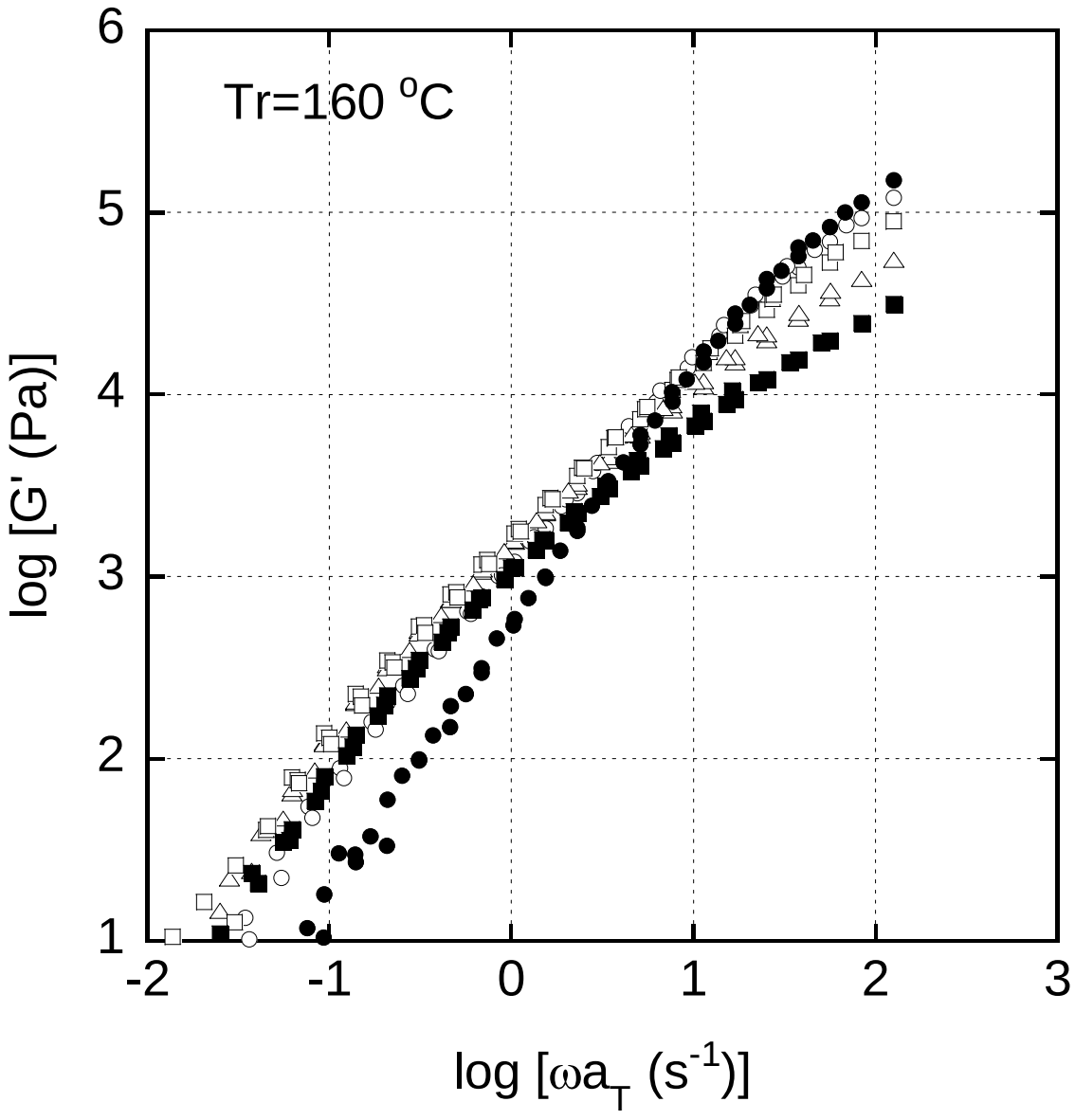

Fig. 2 (b)

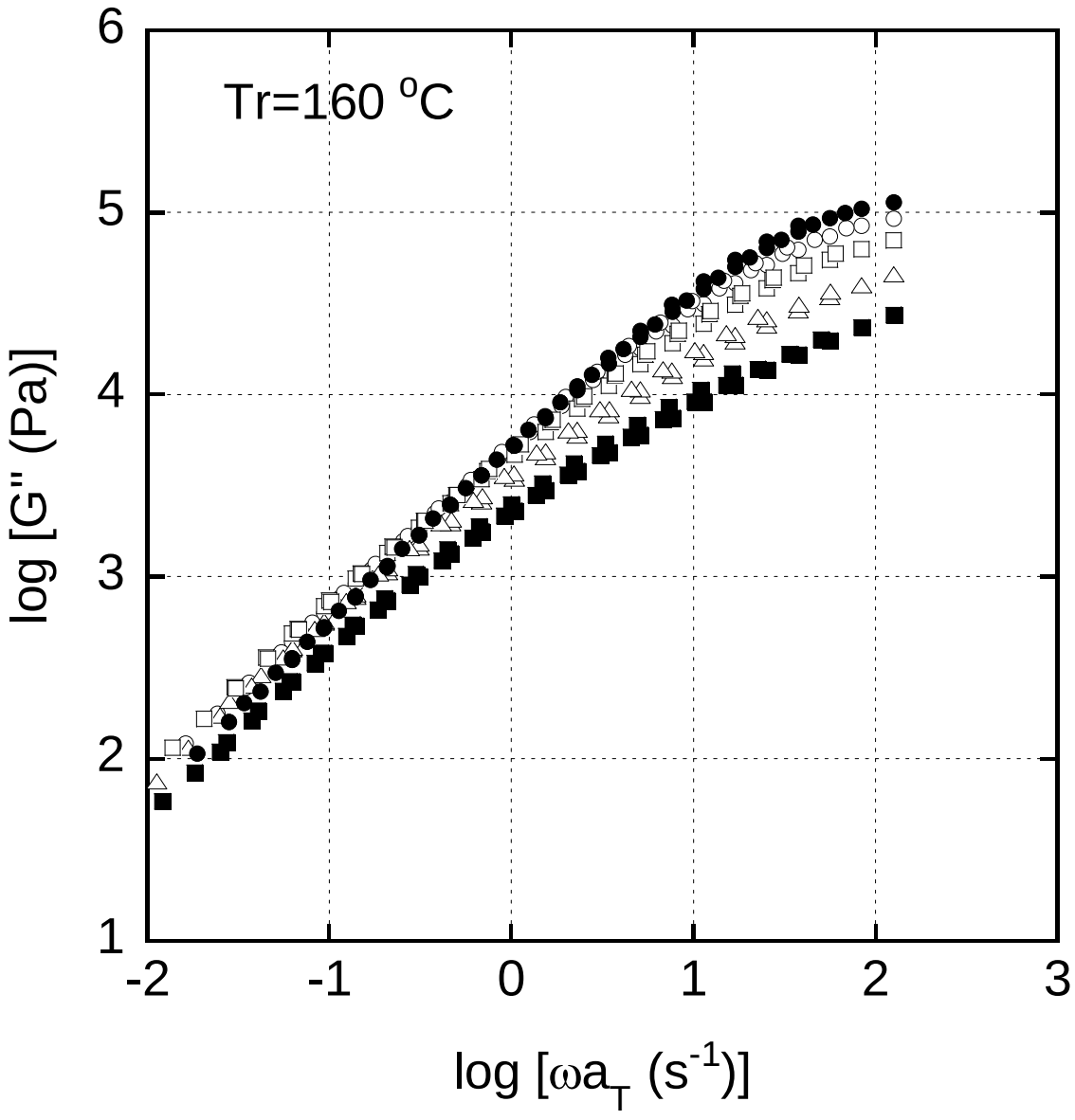

Fig. 3

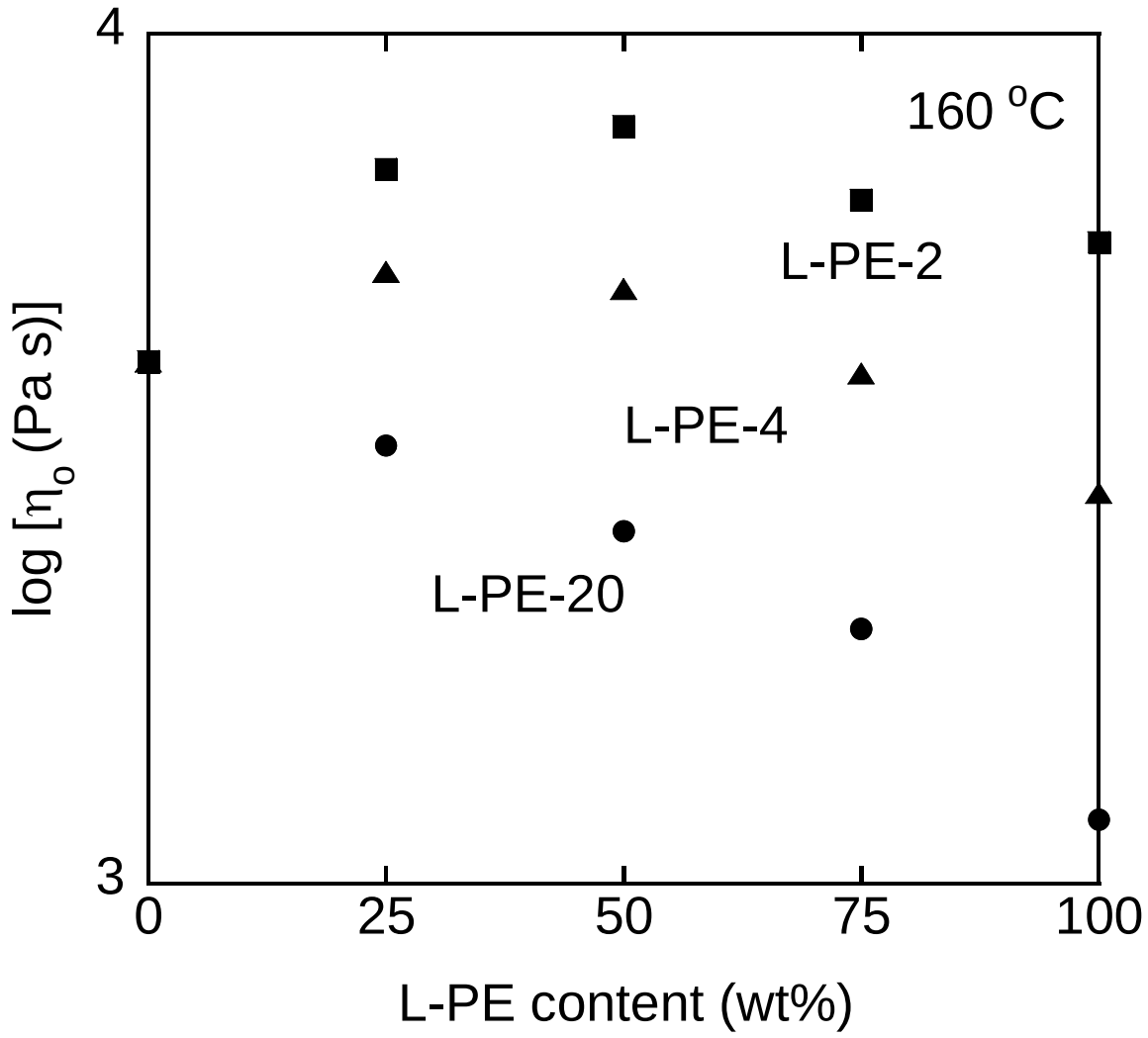

Fig. 4

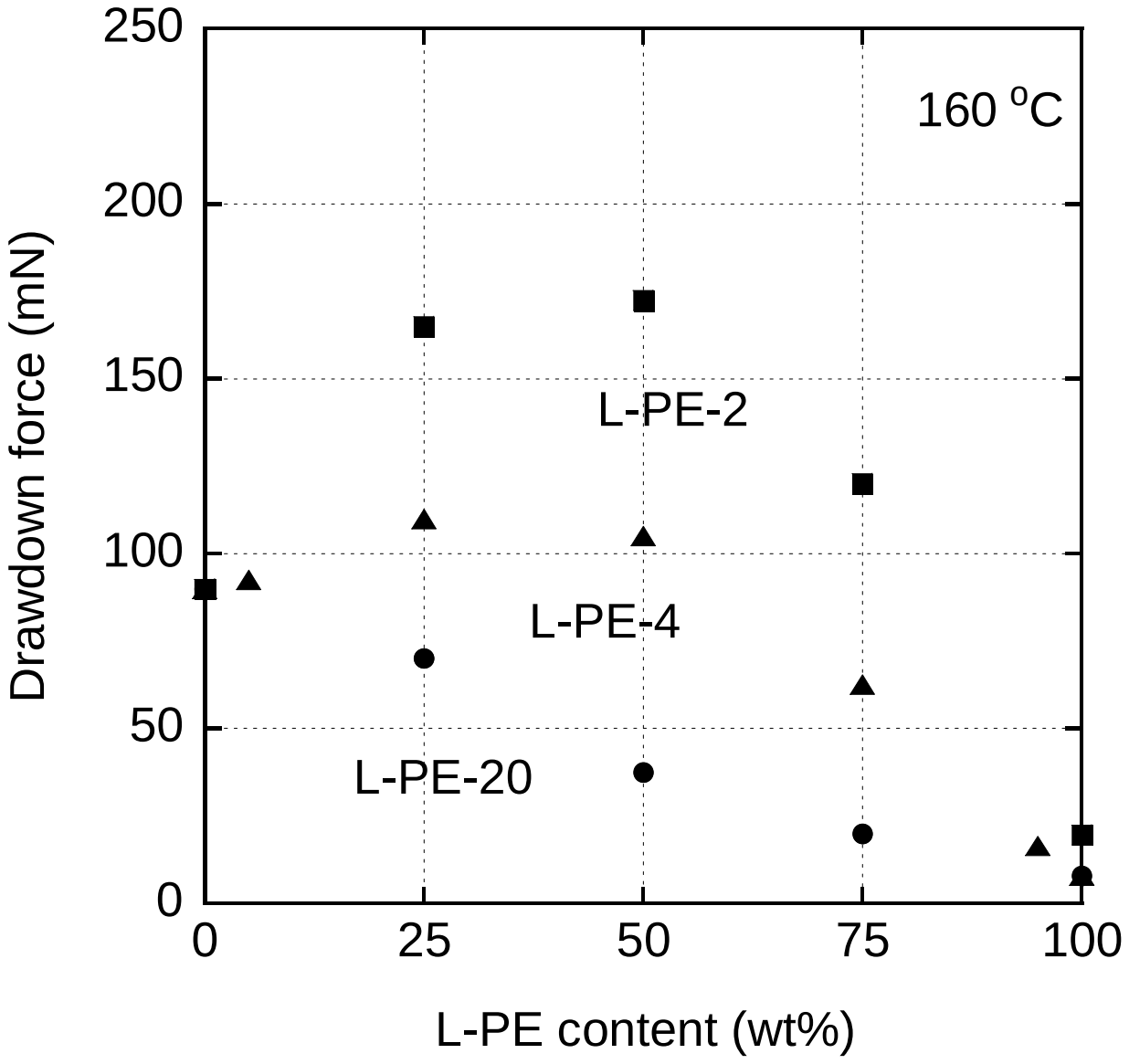
250
200
150
100
50
0
Drawdown force (mN)
160 °C
L-PE-2
L-PE-4
L-PE-20
0
25
50
75
100
L-PE content (wt%)

Fig. 5 (a)

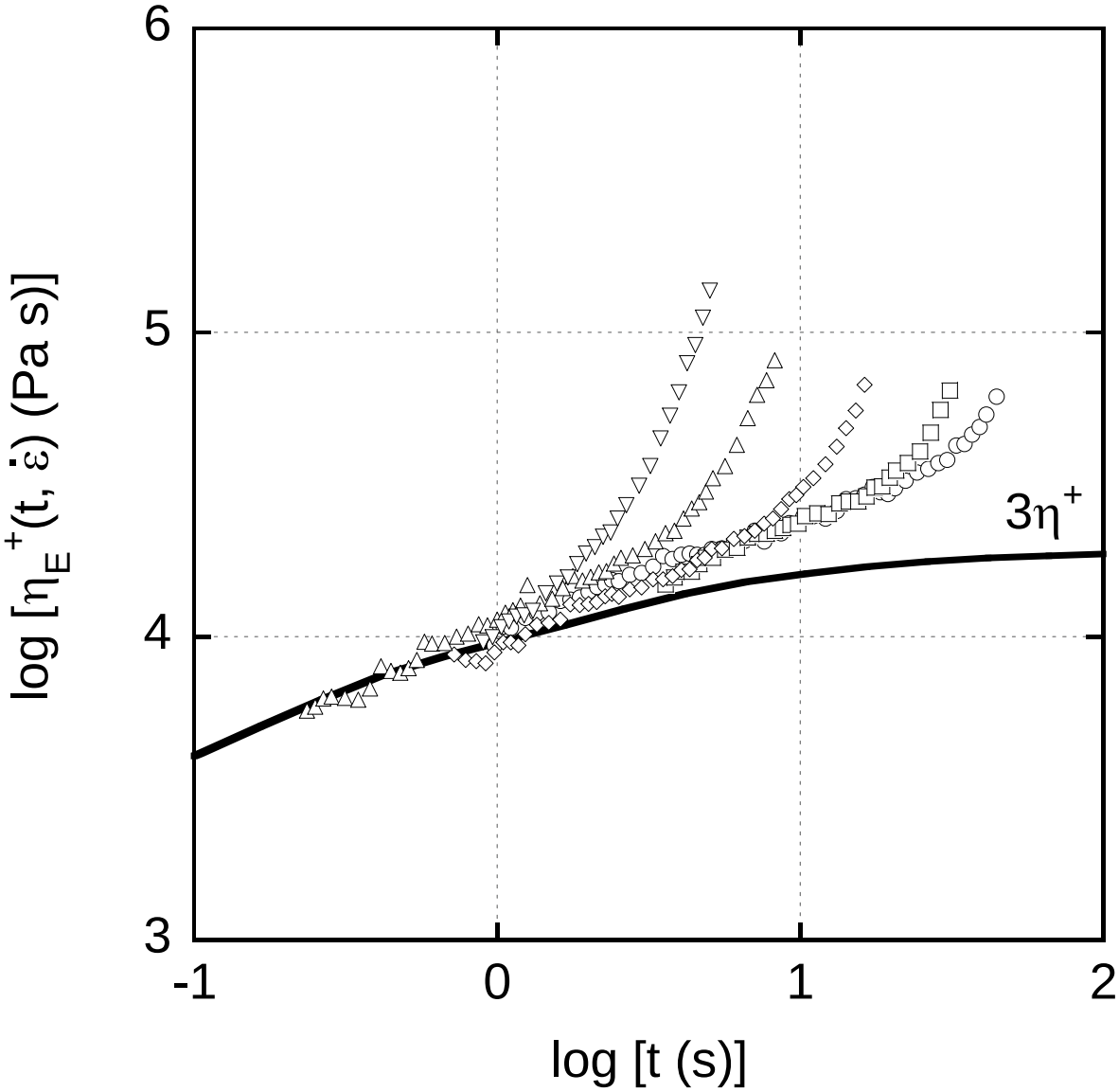

Fig. 5 (b)

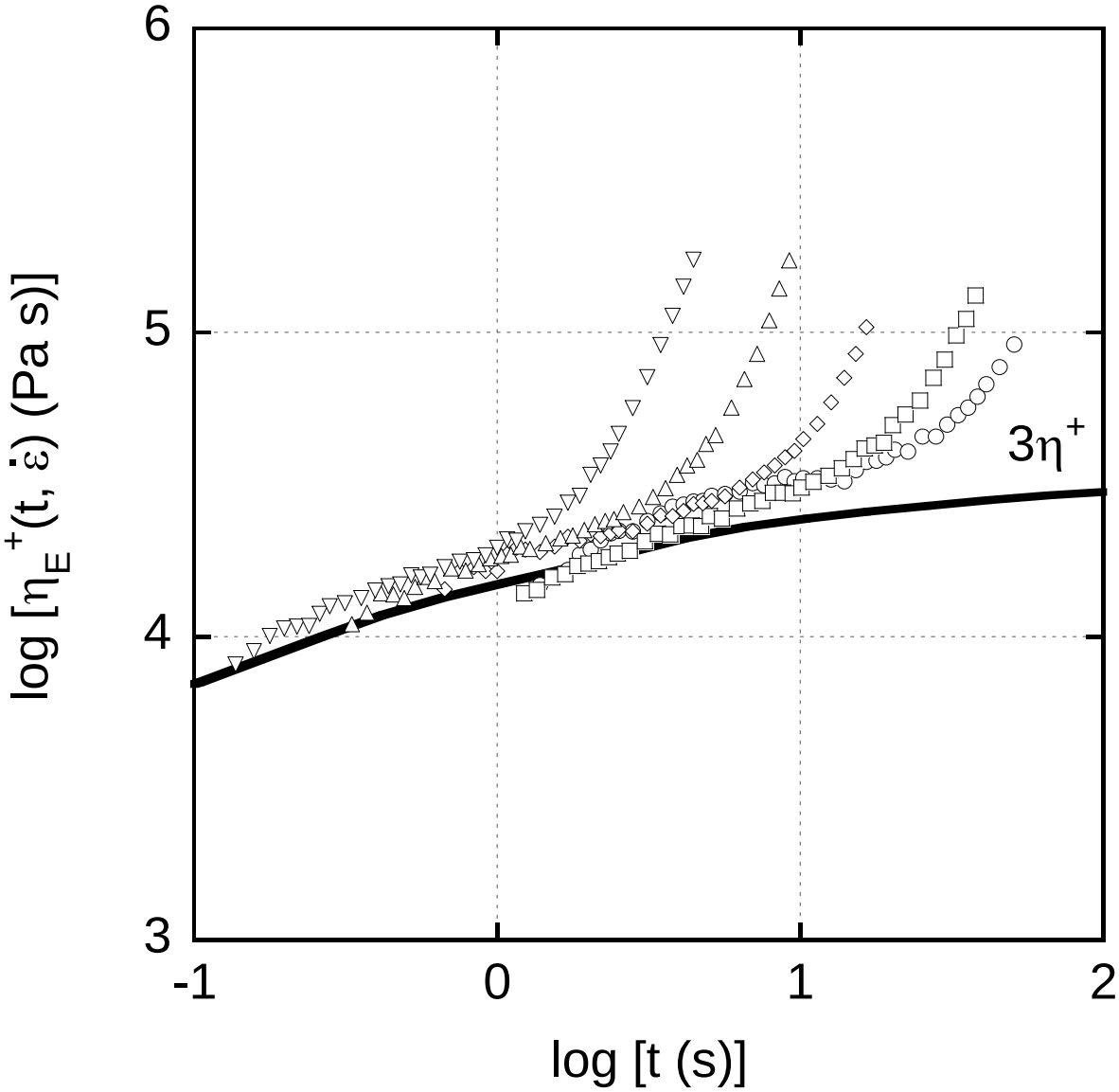

Fig. 5 (c)

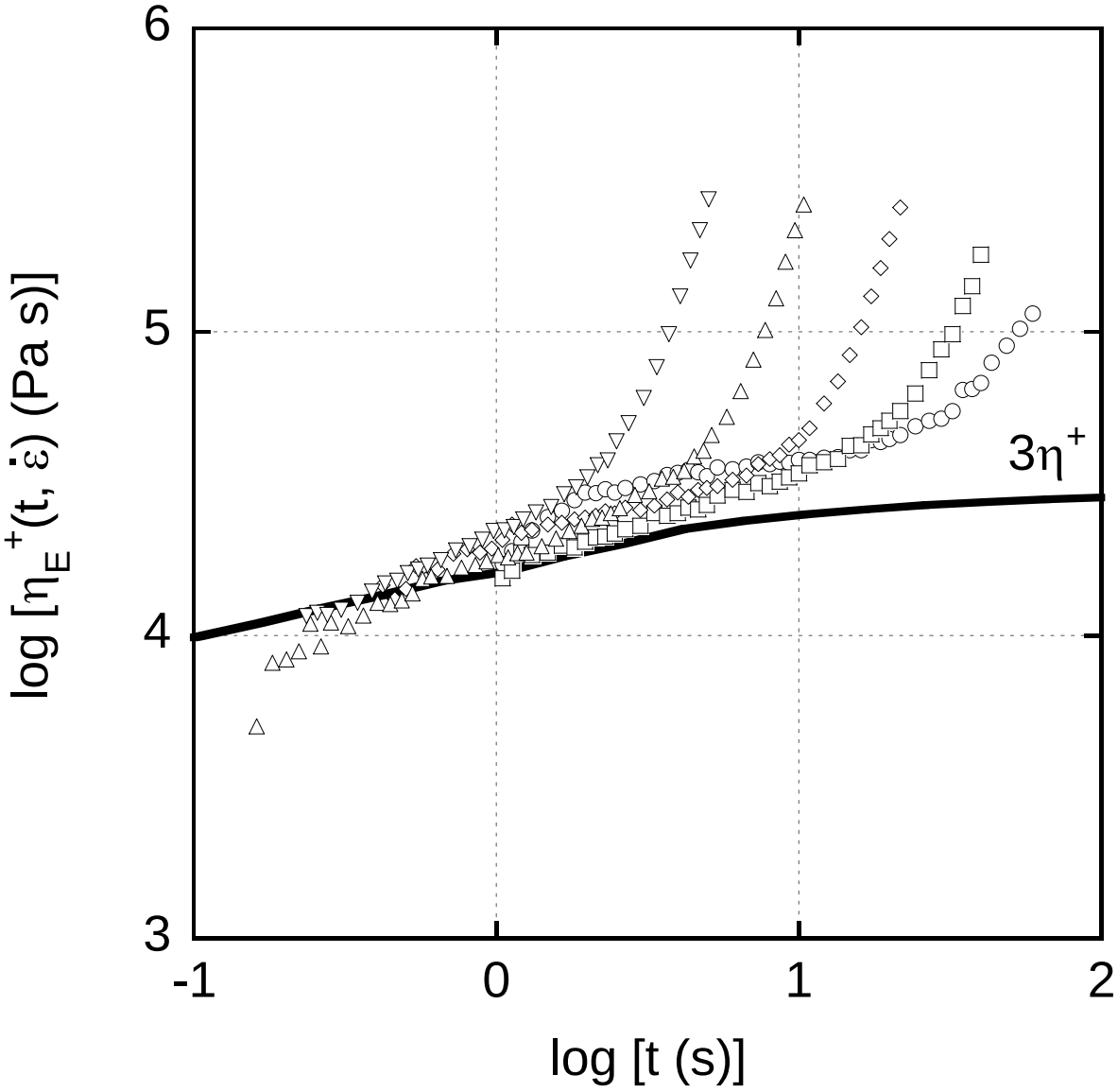

Fig. 5 (d)

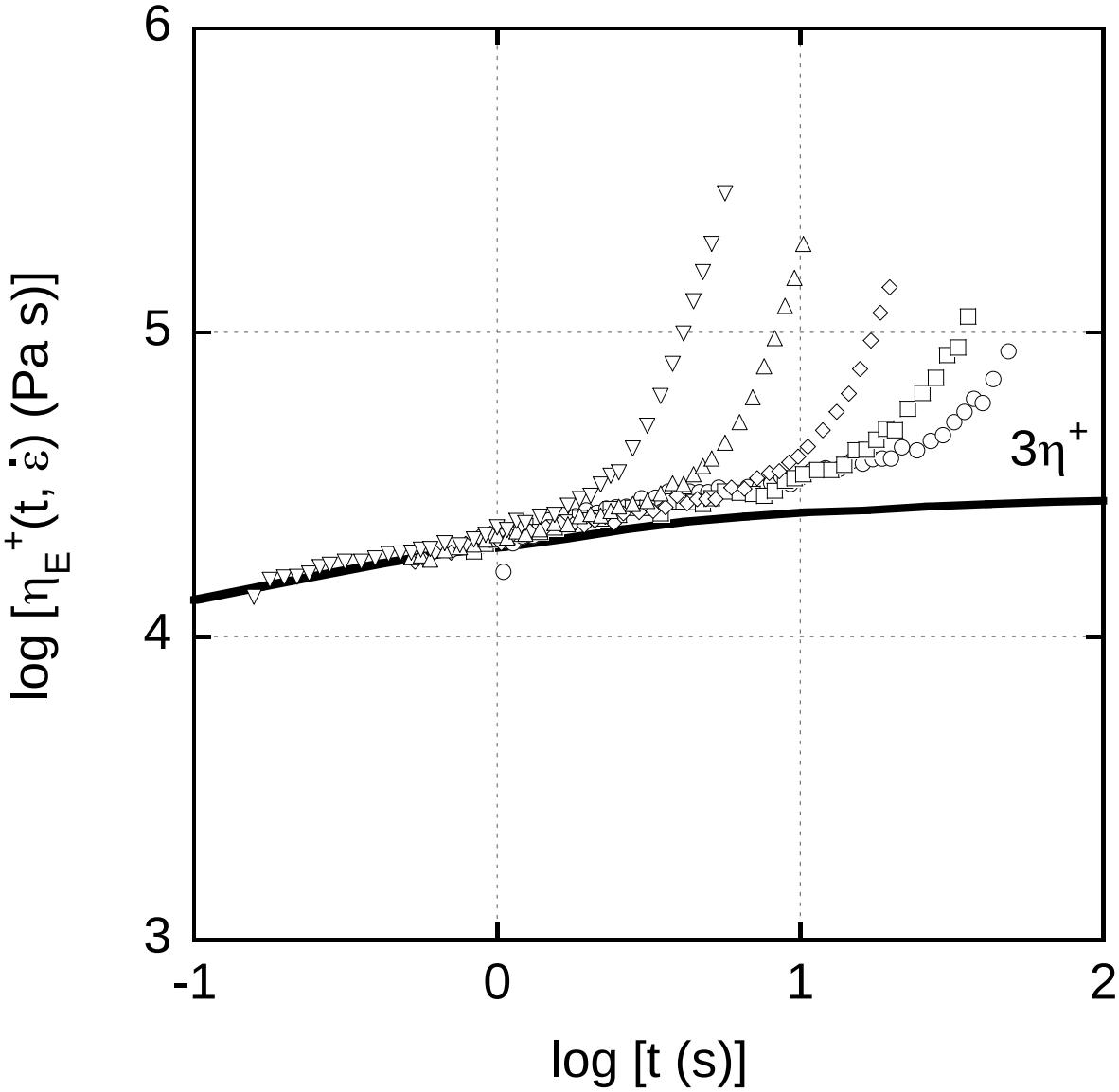

Fig. 5 (e)

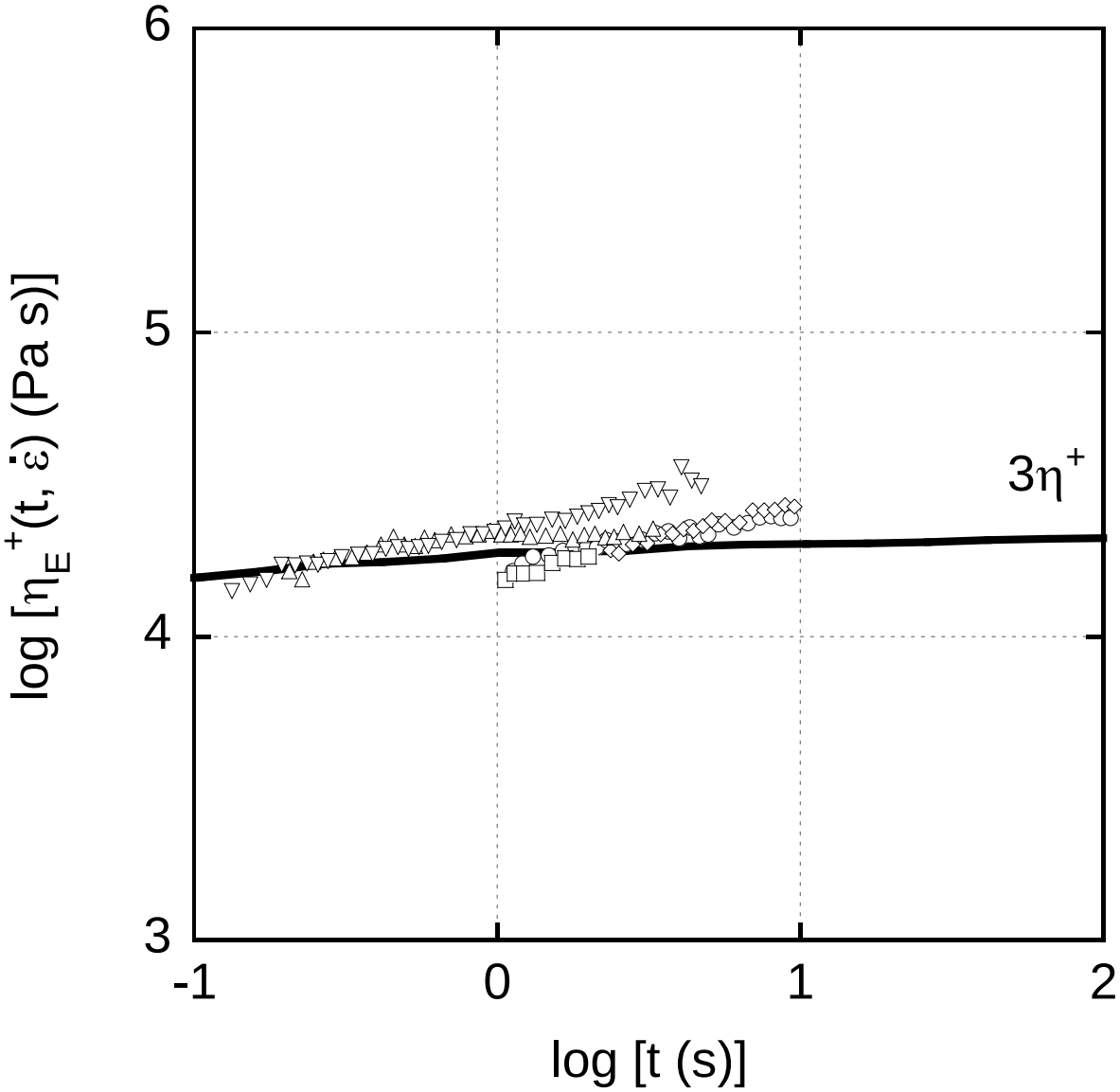

Fig. 6 (a)

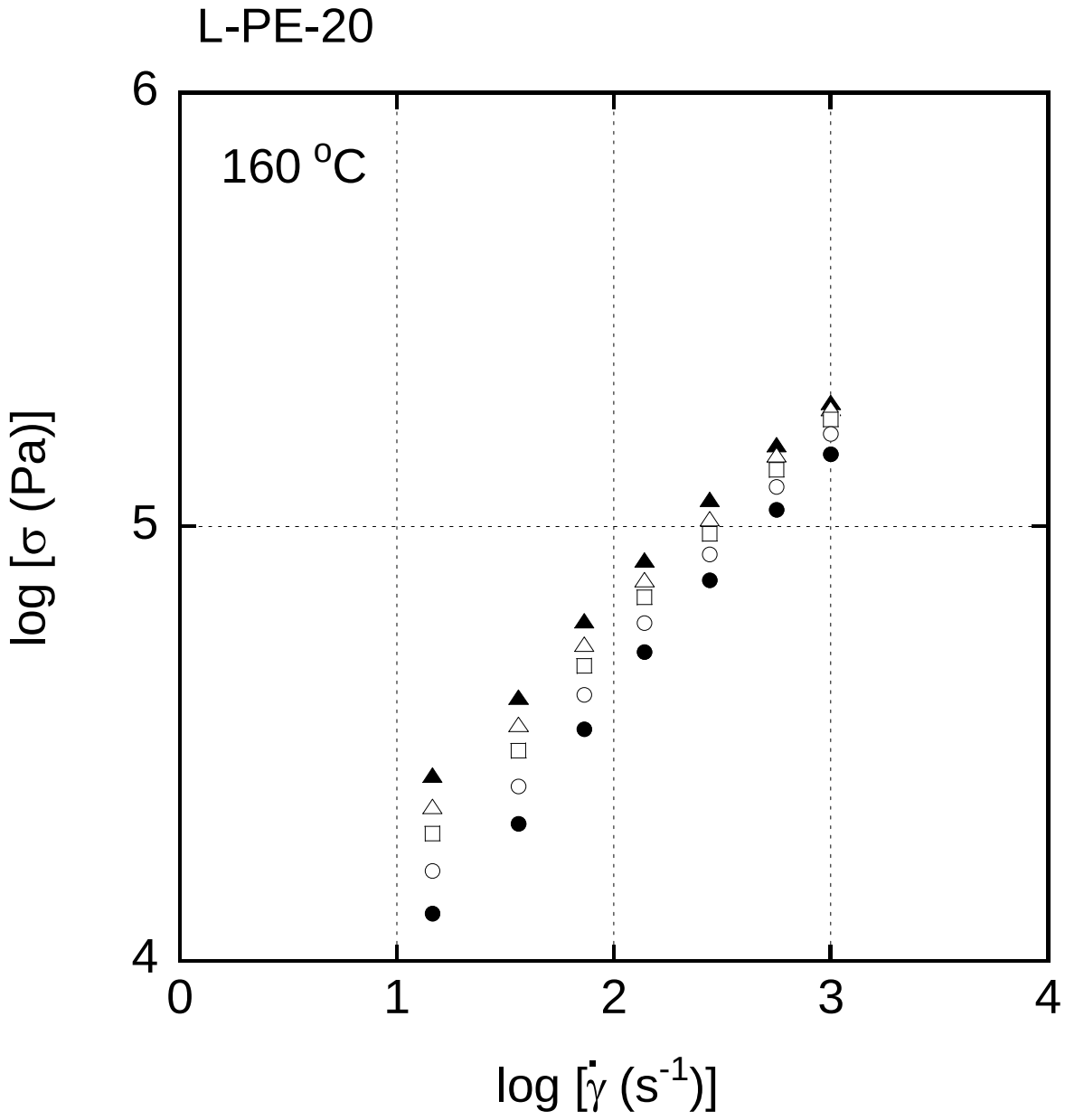

Fig. 6 (b)

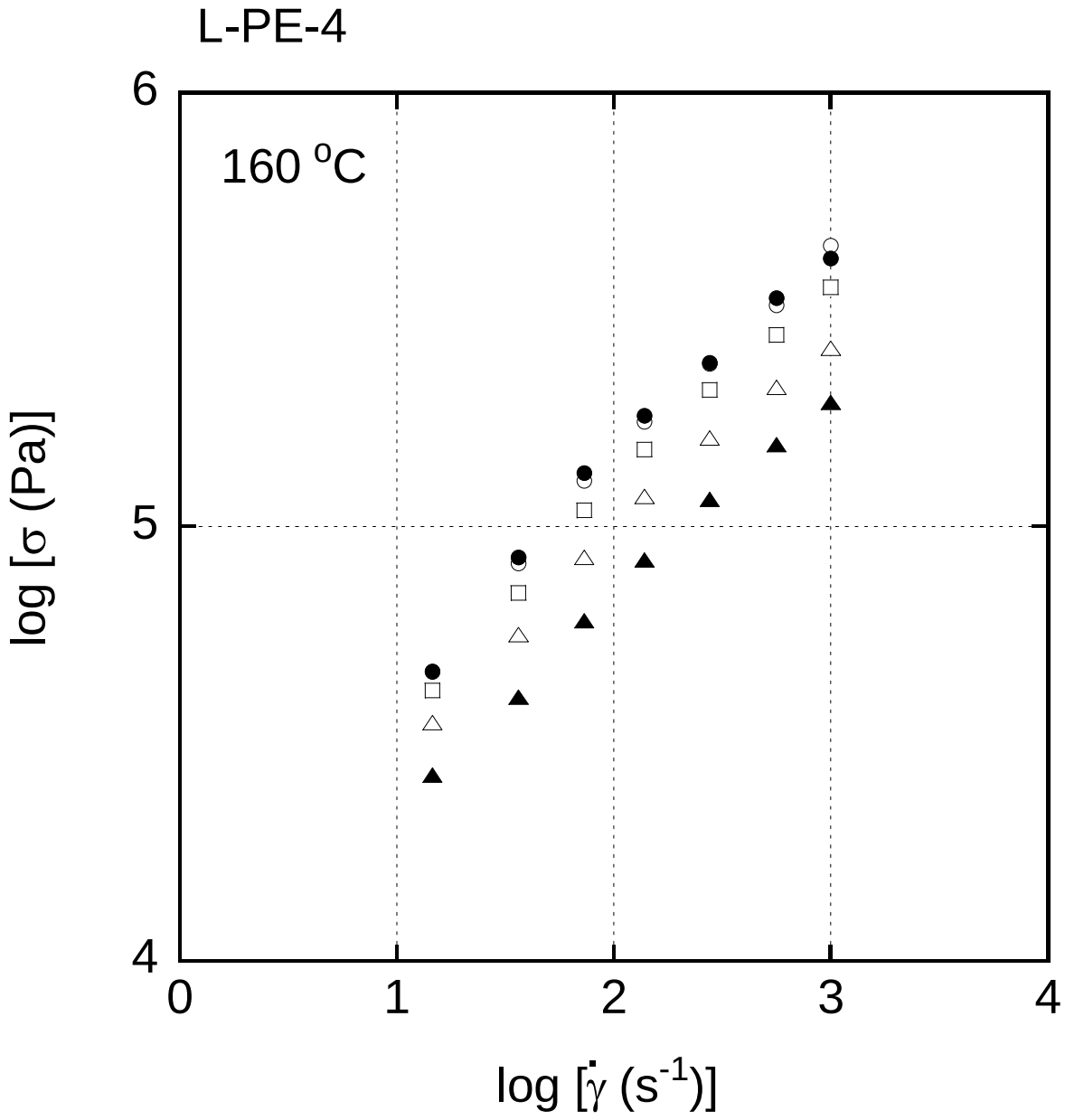

Fig. 6 (c)

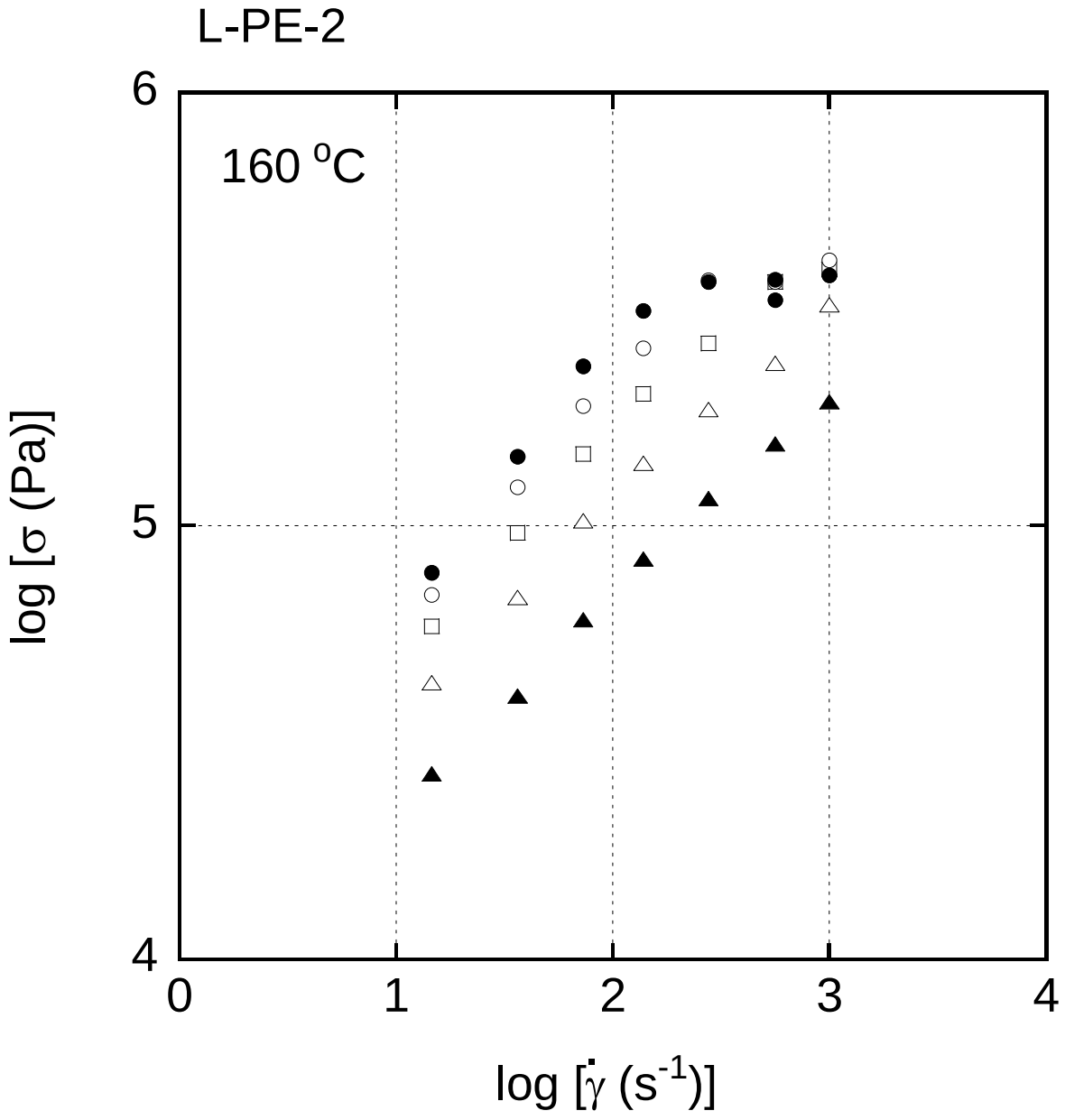

Fig. 7 (a)

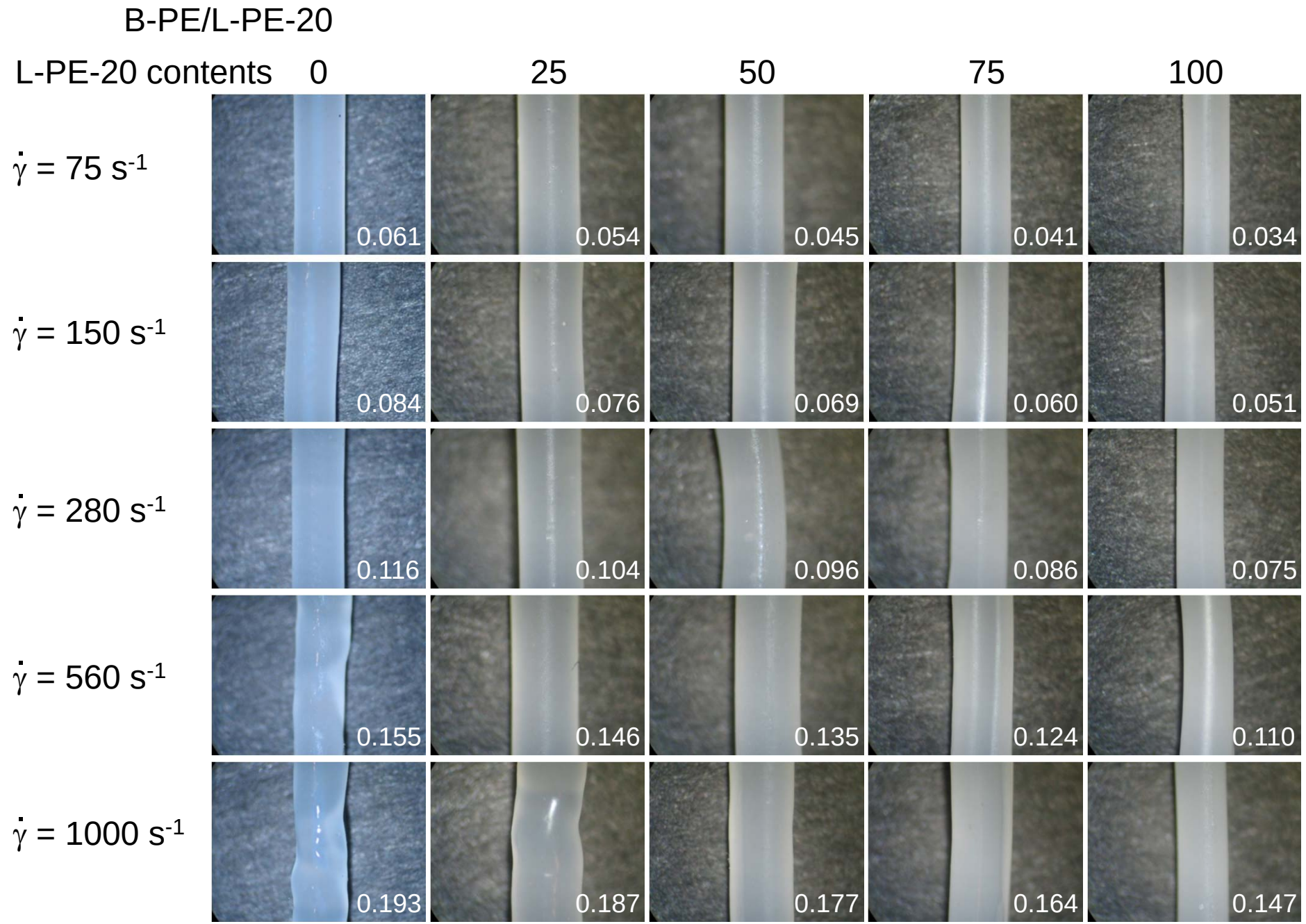
B-PE/L-PE-20
L-PE-20 contents
0
25
50
75
100
$\dot{\gamma}$ = 75 s^{-1}
$\dot{\gamma}$ = 150 s^{-1}
$\dot{\gamma}$ = 280 s^{-1}
$\dot{\gamma}$ = 560 s^{-1}
$\dot{\gamma}$ = 1000 s^{-1}
0.061
0.054
0.045
0.041
0.034
0.084
0.076
0.069
0.060
0.051
0.116
0.104
0.096
0.086
0.075
0.155
0.146
0.135
0.124
0.110
0.193
0.187
0.177
0.164
0.147

Fig. 7 (b)

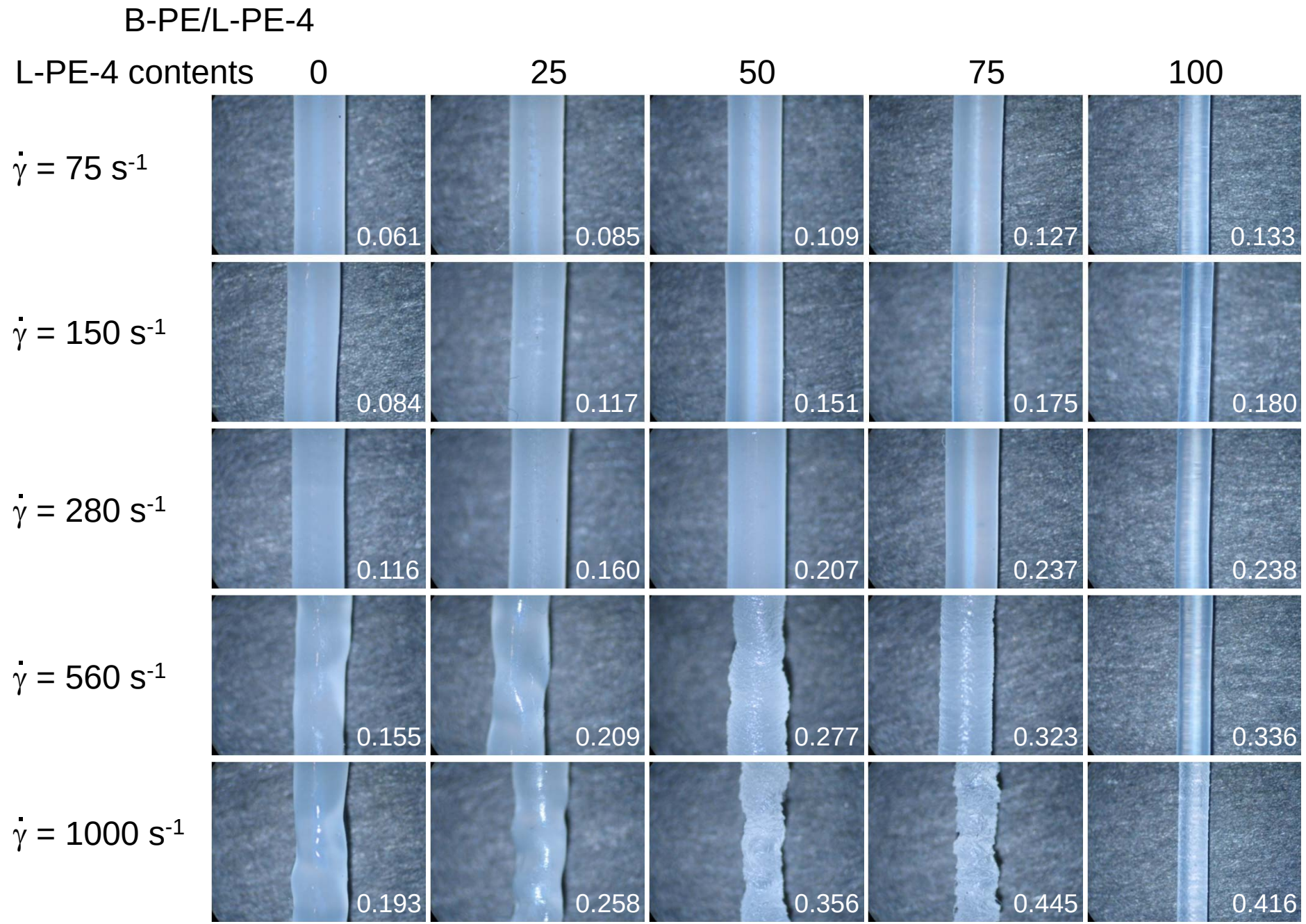
B-PE/L-PE-4
L-PE-4 contents
0
25
50
75
100
$\dot{\gamma}$ = 75 s^{-1}
$\dot{\gamma}$ = 150 s^{-1}
$\dot{\gamma}$ = 280 s^{-1}
$\dot{\gamma}$ = 560 s^{-1}
$\dot{\gamma}$ = 1000 s^{-1}
0.061
0.085
0.109
0.127
0.133
0.084
0.117
0.151
0.175
0.180
0.116
0.160
0.207
0.237
0.238
0.155
0.209
0.277
0.323
0.336
0.193
0.258
0.356
0.445
0.416

Fig. 7 (c)

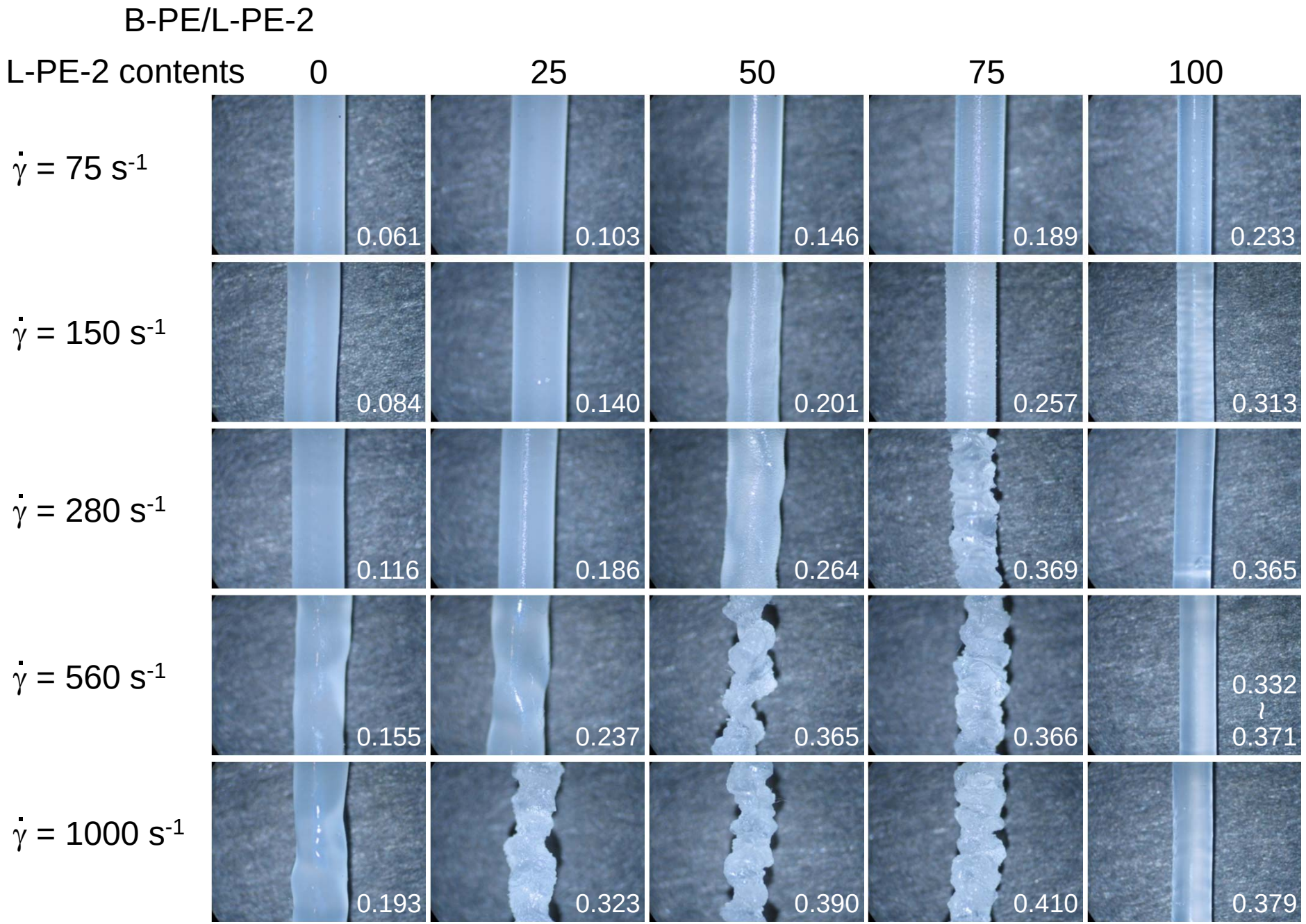
B-PE/L-PE-2
L-PE-2 contents
0
25
50
75
100
$\dot{\gamma}$ = 75 s^{-1}
$\dot{\gamma}$ = 150 s^{-1}
$\dot{\gamma}$ = 280 s^{-1}
$\dot{\gamma}$ = 560 s^{-1}
$\dot{\gamma}$ = 1000 s^{-1}
0.061
0.103
0.146
0.189
0.233
0.084
0.140
0.201
0.257
0.313
0.116
0.186
0.264
0.369
0.365
0.155
0.237
0.365
0.366
0.332
~
0.371
0.193
0.323
0.390
0.410
0.379

Fig. 8

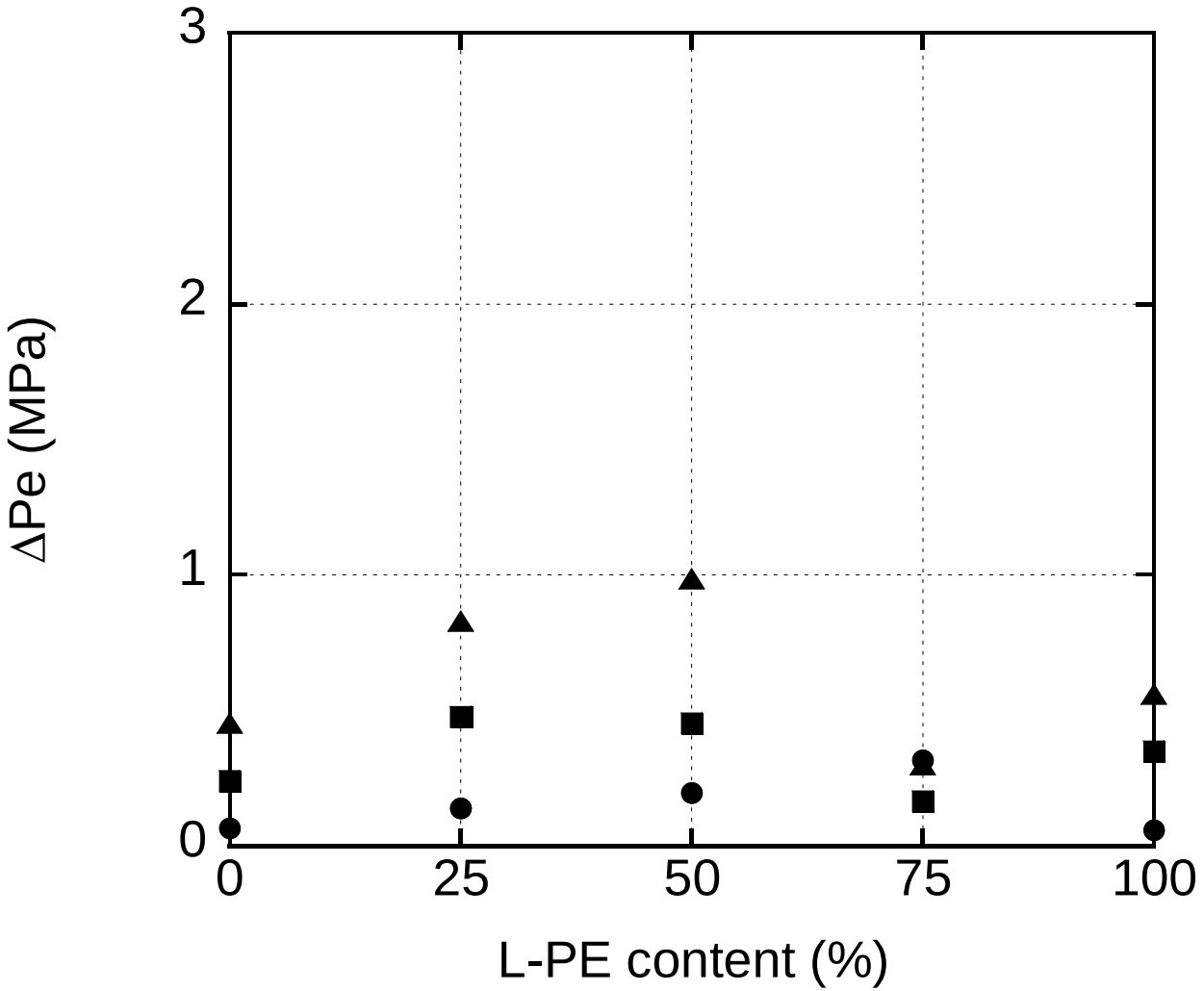

Fig. 9